Early systemic immune biomarkers predict bone regeneration after trauma

Albert Cheng[a,b,1], Casey E. Vantucci[b,c,1], Laxminarayanan Krishnan[b], Marissa A. Ruehle[b,c], Theresa Kotanchek[d], Levi B. Wood[a,b,c], Krishnendu Roy[b,c], and Robert E. Guldberg[a,b,e,2]

[a]George W. Woodruff School of Mechanical Engineering, Georgia Institute of Technology, Atlanta, GA 30332; [b]Parker H. Petit Institute for Bioengineering and Bioscience, Georgia Institute of Technology, Atlanta, GA 30332; [c]Wallace H. Coulter Department of Biomedical Engineering, Georgia Institute of Technology and Emory University, Atlanta, GA 30332; [d]Evolved Analytics LLC, Midland, MI 48640; and [e]Knight Campus for Accelerating Scientific Impact, University of Oregon, Eugene, OR 97403

Edited by Kristi S. Anseth, University of Colorado Boulder, Boulder, CO, and approved January 7, 2021 (received for review September 20, 2020)

Severe traumatic injuries are a widespread and challenging clinical problem, and yet the factors that drive successful healing and restoration of function are still not well understood. One recently identified risk factor for poor healing outcomes is a dysregulated immune response following injury. In a preclinical model of orthopedic trauma, we demonstrate that distinct systemic immune profiles are correlated with impaired bone regeneration. Most notably, elevated blood levels of myeloid-derived suppressor cells (MDSCs) and the immunosuppressive cytokine interleukin-10 (IL-10) are negatively correlated with functional bone regeneration as early as 1 wk posttreatment. Nonlinear multivariate regression also implicated these two factors as the most influential in predictive computational models. These results support a significant relationship between early systemic immune responses to trauma and subsequent local bone regeneration and indicate that elevated circulating levels of MDSCs and IL-10 may be predictive of poor functional healing outcomes and represent novel targets for immunotherapeutic intervention.

immune dysregulation | myeloid-derived suppressor cell | trauma | bone regeneration

Musculoskeletal trauma involving extremities is quite common, occurring in up to 71% of battlefield injuries (1) and 59% of civilian injuries (2). Despite advances in treatment, failure of bone healing continues to be a significant clinical concern. A large population study found a 4.9% overall risk of nonunion for fractures and even higher risk depending on anatomic location and patient comorbidities (3). Furthermore, in patients with severe lower extremity trauma who underwent limb salvage, a nonunion rate of 31% has been reported (4), highlighting the dramatic increase in nonunion risk as trauma complexity increases. Recent studies have also identified a dysregulated immune response, including chronic immunosuppression and immune paralysis, as an important cause of morbidity following severe trauma (5–7).

It has been hypothesized that trauma-induced immune dysregulation occurs in multiple stages. The first stage encompasses a systemic inflammatory response syndrome (SIRS), characterized by acute hyperinflammation with overproduction of proinflammatory cytokines (interleukin [IL]-1, IL-6, tumor necrosis factor [TNF] α), countered by a compensatory anti-inflammatory response syndrome (CARS) with increased expression of anti-inflammatory cytokines (IL-1RA, IL-10, transforming growth factor [TGF] β) (8). CARS follows almost immediately after initiation of SIRS, as prolonged exposure to the high levels of inflammatory factors and reactive oxygen species generated during SIRS is damaging to the surrounding tissues and can lead to multiple organ failure if left unchecked (9, 10). In most cases of uncomplicated healing, the SIRS and CARS responses resolve, and systemic immune homeostasis is restored within a couple of weeks. Failure to achieve this balance can lead to a storm of elevated proinflammatory and anti-inflammatory signals that persists for several weeks (11) and can eventually result in a destructive catabolic phase (12), characterized by the onset of systemic immune dysregulation and immune suppression (SIDIS) (13). Patients exhibiting symptoms of SIDIS are more prone to opportunistic infections, sepsis, organ dysfunction, and often require multiple surgical interventions and hospitalizations, incurring greater long-term healthcare costs (12, 14).

The primary cellular mediators of long-term immune dysregulation observed in SIDIS are immune suppressor cell types, including T regulatory cells and myeloid-derived suppressor cells (MDSCs) (6, 7, 14). These cells suppress immune function by secreting anti-inflammatory factors, such as IL-1RA, IL-10, and TGFβ, which can subsequently inhibit activation of other immune cells, such as in T cell anergy, or even reduce immune populations over time by promoting premature apoptosis of these cells (14–16). MDSCs in particular are immature myeloid lineage cells that are distinct from other myeloid immune cells, such as macrophages, granulocytes, and dendritic cells (17). Additionally, MDSCs are heterogeneous in nature and most commonly identified in rats as expressing both neutrophil (His48) and monocyte (CD11b) markers (18, 19). These cells can directly suppress T cell function through depletion of the amino acid L-arginine (15, 20), which is a critical mediator of T cell metabolism and activity (21), as well as through promotion of nitric oxide-mediated T cell apoptosis (18). MDSCs are also involved in

Significance

Chronic nonunion following traumatic bone injury remains a challenging clinical problem, and delayed treatment of an established nonunion is associated with variable outcomes and often prolonged patient disability. Here we used a rodent model of nonunion with delayed treatment to investigate the factors that influence effective healing. We found that certain immune profiles are linked to impaired bone regeneration. In particular, increased early levels of myeloid-derived suppressor cells and the cytokine interleukin-10 in blood are predictive of subsequent poor healing outcomes. These results suggest that the early systemic immune response to trauma can help predict the long-term effectiveness of bone healing treatments and may inform the development of immunotherapies for orthopedic repair.

Author contributions: A.C., C.E.V., L.K., K.R., and R.E.G. designed research; A.C., C.E.V., L.K., and M.A.R. performed research; T.K. contributed new reagents/analytic tools; A.C., C.E.V., T.K., L.B.W., K.R., and R.E.G. analyzed data; and A.C. and C.E.V. wrote the paper.

The authors declare no competing interest.

This article is a PNAS Direct Submission.

[1]A.C. and C.E.V. contributed equally to this work.

[2]To whom correspondence may be addressed. Email: guldberg@uoregon.edu.

This article contains supporting information online at https://www.pnas.org/lookup/suppl/doi:10.1073/pnas.2017889118/-/DCSupplemental.

Published February 17, 2021.

TGFβ1-mediated suppression of natural killer cells (22) and can enhance T regulatory cell survival (23, 24). In human patients, circulating MDSCs have been observed to persist at high levels up to 28 d in severely septic patients and have been linked to adverse outcomes and prolonged intensive care unit stays (16). However, the influence of MDSCs following traumatic musculoskeletal injuries, particularly in cases of poor healing, such as bone fracture nonunion, remains unclear.

Here we used a previously established femoral bone defect model of chronic nonunion in rats (25) to investigate systemic immune dysregulation and how it relates to functional bone regeneration. In this model, treatment with bone morphogenetic protein 2 (BMP-2) is delivered 8 wk after initial creation of the bone defect (delayed treatment), which is the time needed to establish nonunion, as defined by radiographic mineralized capping of bone ends. This delayed treatment group mirrors the clinical standard of care, given that nonunion is not diagnosed and reintervention is not performed until several months after the initial injury (26). Acute treatment (i.e., treatment delivered immediately following defect creation) was also investigated and represents an example of a relatively uncomplicated bone healing scenario. We hypothesized that delayed treatment would result in poor bone healing compared to acute treatment, and, furthermore, that this impairment could be linked to systemic immune dysregulation involving increases in immunosuppressive cell types and cytokines and simultaneous decreases in immune effector cells and cytokines.

Systemic immune characterization was performed on blood samples collected longitudinally over multiple weeks (*SI Appendix*, Fig. S1) to investigate immune profile changes during healing. Blood collected at each time point was analyzed for immune cell populations by flow cytometry as well as for serum cytokines and chemokines through a multiplexed array. These results were evaluated concurrently with bone healing, which was quantified by in vivo micro computed tomography (μCT) and ex vivo biomechanical testing of the regenerated femurs. Finally, univariate and multivariate analyses were performed to develop computational predictive models of bone healing based on the blood immune cell and cytokine data.

Results

Functional Regeneration Is Impaired following Delayed Treatment of Bone Defects. Bone regeneration and mechanics were significantly decreased with delayed treatment. Longitudinal radiographs showed progression of bone healing following delayed and acute treatment with BMP-2 (Fig. 1*A*). While both groups exhibited increased bone formation over time, the defects that received delayed treatment had qualitatively less bone than the acutely treated defects, particularly in the center of the newly regenerated defect. This observation was supported by the μCT reconstructions of the new bone at 20 wk (Fig. 1*B*), which demonstrated more void space within the bone defect in the delayed treatment group. Quantification of new bone formation by μCT revealed that the acutely treated defects had significantly higher bone volumes at both weeks 14 and 20 (Fig. 1*C*). No differences were observed in local bone mineral density (Fig. 1*D*). Furthermore, biomechanical testing demonstrated that delayed treatment resulted in regenerated bones with lower mechanical strength and stiffness (Fig. 1 *E* and *F*) compared to acute treatment. Additionally, acute treatment resulted in complete restoration of intact bone stiffness, whereas defects receiving delayed treatment recovered on average only 32% of the intact bone stiffness. In terms of bone strength, acutely treated defects were over twice as strong as delayed treated defects, demonstrating a significant detrimental effect of delayed treatment on functional regeneration.

Circulating and Local Immune Cells Correlate with Bone Regeneration. Immune cell characterization from blood was performed at multiple time points (Fig. 2 *A*–*G*). No significant differences were observed between acute and delayed treatment for all cell types evaluated.

However, linear regression analysis revealed several significant correlations with respect to week 20 bone volumes (Fig. 3 *A*–*E*). A table of the linear regression statistics can be found in *SI Appendix*, Table S1). Immunosuppressive MDSCs and monocytes in blood were negatively correlated with bone healing at multiple timepoints posttreatment (Fig. 3 *A* and *B*). Of note, blood MDSC levels were significantly negatively correlated as early as week 9, or 1 wk posttreatment. In contrast, the immune effector T cells, including the T helper cell subset, and B cells in blood were positively correlated with bone healing (Fig. 3 *C*–*E*). Interestingly, blood B cells were significantly correlated at weeks 1 and 4 following trauma, several weeks before the delayed BMP-2 treatment was administered at week 8. Independent analyses of local tissues harvested at week 20 demonstrated consistent correlations with the blood immune response profiles; MDSCs in the bone marrow were negatively correlated with healing, while B cells in the muscle tissue adjacent to the defect were positively correlated (*SI Appendix*, Fig. S2).

Multivariate Analysis Identifies Immune Cells and Cytokines Associated with Healing. Using the blood immune cell and cytokine data for all time points pooled together (weeks 0 through 20), partial least squares regression (PLSR) was performed to identify the most influential factors during the entire course of the study. This analysis revealed an axis, termed latent variable 1 (LV1), that successfully describes the gradient of observed healing responses as defined by bone volume (Fig. 4*A*). The LV1 profile shows factors that are elevated (positive bars) and diminished (negative bars) with respect to bone healing (Fig. 4*B*). In agreement with the conventional linear regression results, MDSCs and monocytes were most negatively correlated with bone healing, while B cells were most positively correlated. Furthermore, IL-6 and IL-13 were the top cytokine correlates with successful healing.

Myeloid-Derived Suppressor Cells Are an Early Indicator of Poor Healing. Pooled analyses of all time points provided broad insight into factors that are most influential during the entire timespan of healing; however, early markers posttreatment are most useful for clinical prediction of treatment success and bone healing outcomes, so we next performed univariate and multivariate analyses of the immune cells and cytokines at week 9, just 1 wk posttreatment. Across the week 9 samples, we observed a spectrum of different immune cell and cytokine responses, as visualized on the heatmap in Fig. 5*A*. Univariate analyses revealed that only the cytokines interferon gamma-induced protein 10 (IP-10), IL-1β, and IL-10 exhibited significant correlations with bone volume, with all having negative correlations (*SI Appendix*, Fig. S3). The multivariate PLSR was able to segregate the week 9 samples by bone volume using a new LV1 (Fig. 5*B*); this LV1 profile shows the week 9 factors that are positively or negatively correlated with long-term bone healing (Fig. 5*C*), several of which overlap with those identified by the PLSR of the pooled time points. In support of the previous results, MDSCs and monocytes were most negatively correlated with bone healing, while B cells, T helper cells, and all T cells were most positively correlated. Furthermore, cytokines IP-10, IL-1β, and IL-10 were negatively correlated with healing, while IL-13 and IL-6 were positively correlated with healing.

Nonlinear Multivariate Regression Further Supports MDSCs and IL-10 as Early Negative Predictors of Bone Healing. Finally, nonlinear regression was performed independently using Evolved Analytics DataModeler software to further evaluate the week 9 immune cells and cytokines. This approach has an advantage over linear regression methods by making fewer a priori assumptions about

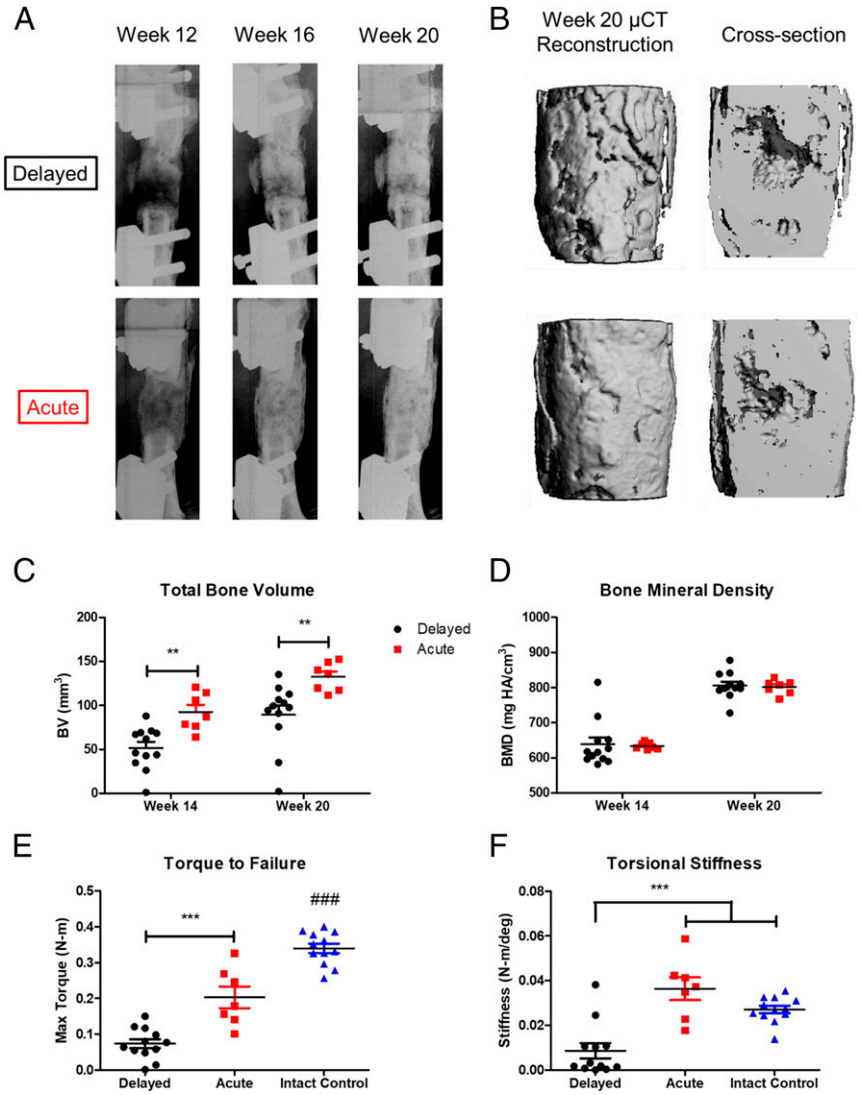

Fig. 1. Functional regeneration is impaired following delayed treatment of bone defects. (*A*) Representative radiographs (median healing sample for each treatment group) demonstrating bone formation at weeks 12, 16, and 20 (corresponding to 4, 8, and 12 wk posttreatment). (*B*) Week 20 μCT reconstructions of the same representative sample and the associated cross-sectional view. (*C* and *D*) Total bone volume (*C*) and bone mineral density (*D*) for the newly formed bone, as quantified by in vivo μCT. (*E* and *F*) Mechanical strength (*E*) and stiffness (*F*) of the regenerated femurs were determined by ex vivo torsional testing to failure at week 20. Data are mean ± SEM, $n = 8$ to 12/group. $^{**}P < 0.01$; $^{***}P < 0.001$ as indicated; $^{###}P < 0.001$ vs. all other groups.

model form. More than 1,100 unique models were generated using this computational approach, and from these, only 191 were selected as the fittest models (Fig. 6*A*). The variable distribution of the selected models was subsequently analyzed (Fig. 6*B*), which revealed the presence of MDSCs and IL-10 in >90% of these models. Furthermore, models involving the top variable combination of MDSCs, IL-10, and RANTES were chosen and aggregated into a predictive model ensemble. This model ensemble represents the collection of models that best maximize diversity of the error residuals for the week 9 data, and further analysis of the ensemble variable response plots (Fig. 6*C*) showed that MDSCs and IL-10 were negatively correlated with bone volume, while RANTES was positively correlated with bone volume. Interestingly, the MDSC response plot demonstrated a distinct nonlinear behavior with respect to bone volume, whereas IL-10 and RANTES both exhibited a more linear response. Finally, the model ensemble bone volume predictions were compared to the observed bone volumes for all samples (Fig. 6*D*) and demonstrated high predictive power based on just the three variable inputs of MDSCs, IL-10, and RANTES ($R^2 = 0.9255$).

Discussion

Systemic immune dysregulation has recently emerged as an important clinical consideration following severe trauma, even in the absence of sepsis or multiple organ failure. Efforts toward identifying predictive biomarkers and better diagnostics for disorders like SIDIS are still in the nascent stages (14). Furthermore, the influence of systemic immune dysregulation on bone repair has yet to be directly investigated, particularly in poor healing outcomes such as nonunion. Here we sought to address these substantial clinical and scientific gaps.

This work demonstrates long-term immune dysregulation in a preclinical model of chronic nonunion, a serious orthopedic complication that remains challenging to treat. In support of our hypothesis, we observed that acute treatment with BMP-2 resulted in improved healing compared to equivalent delayed treatment after nonunion has been established. We did not observe outright differences between the acute and delayed treatment groups in the individual immune cell populations or cytokine levels at any time point; however, differences may have been hard to discern by simple comparative analyses, due to the redundant and pleiotropic

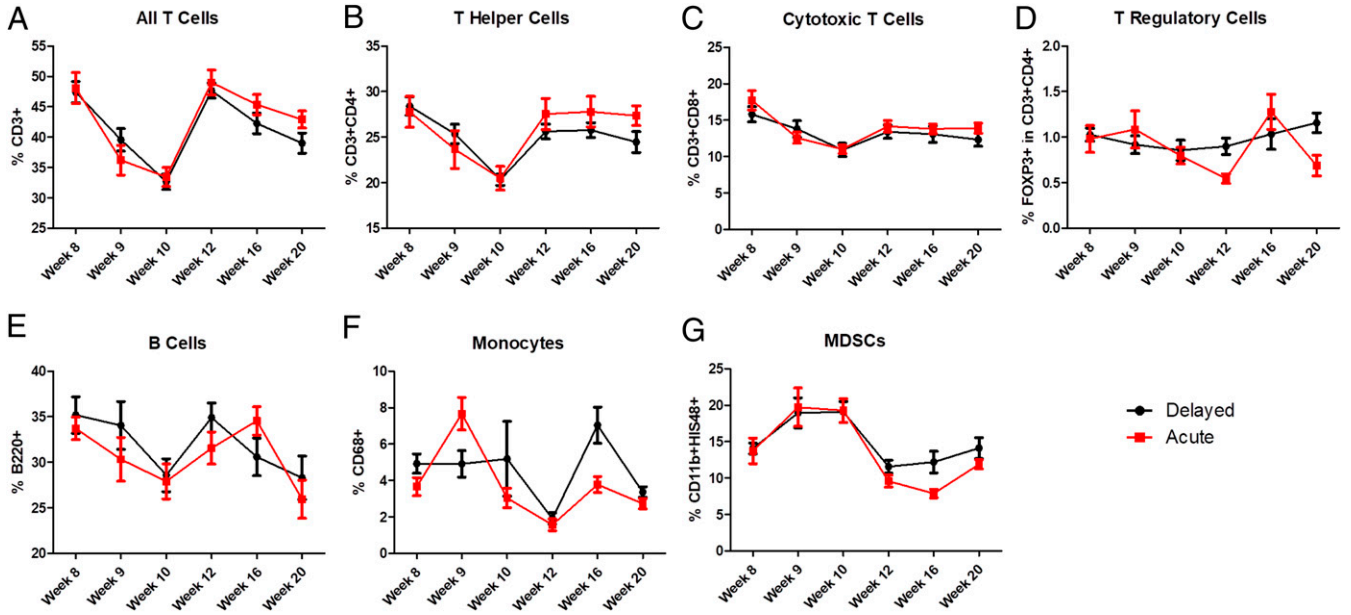

Fig. 2. Longitudinal characterization of circulating immune cells. (*A*–*G*) No significant differences between delayed and acute groups were observed in circulating immune cell populations from week 8 (baseline immediately before treatment) through week 20 (12 wk posttreatment). Mean ± SEM, $n = 8$ to 12/group.

effects of these factors. Correlative analyses utilizing univariate and multivariate methods may be more appropriate and insightful. Univariate analyses of immune cells in blood at multiple time points revealed a significant negative correlation between MDSCs and long-term bone regeneration, as early as weeks 9 and 10 (1 and 2 wk posttreatment, respectively). In contrast, B cells, T cells, and T helper cells were positively correlated with bone repair. These results suggest that impaired bone healing in this model involves a systemic rise in MDSCs that coincides with reductions in effector B and T cell populations, consistent with previously reported profiles of chronic systemic immune dysregulation associated with infection and cancer (17, 20, 27).

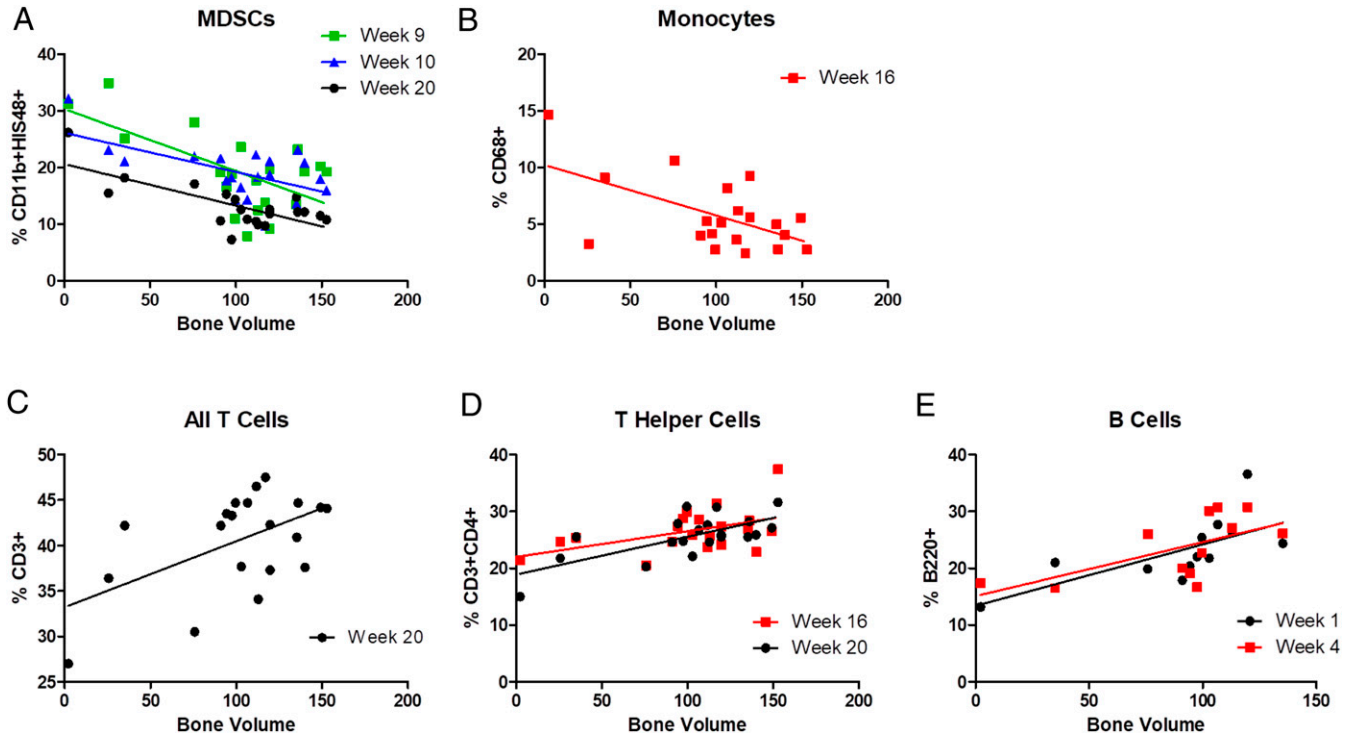

Fig. 3. Circulating immune cells correlate with bone regeneration. (*A*–*E*) Select cell populations from peripheral blood demonstrated a significant correlation with week 20 bone volumes. MDSCs and monocytes were negatively correlated with bone healing (*A* and *B*), while T cells, T helper cells, and B cells were positively correlated (*C*–*E*). The positive B cell correlations observed at weeks 1 and 4 are notable, given that they occurred several weeks before BMP-2 treatment was administered at week 8. $n = 12$ to 20 per time point, slope of linear regression significantly nonzero for all data shown; $P < 0.05$.

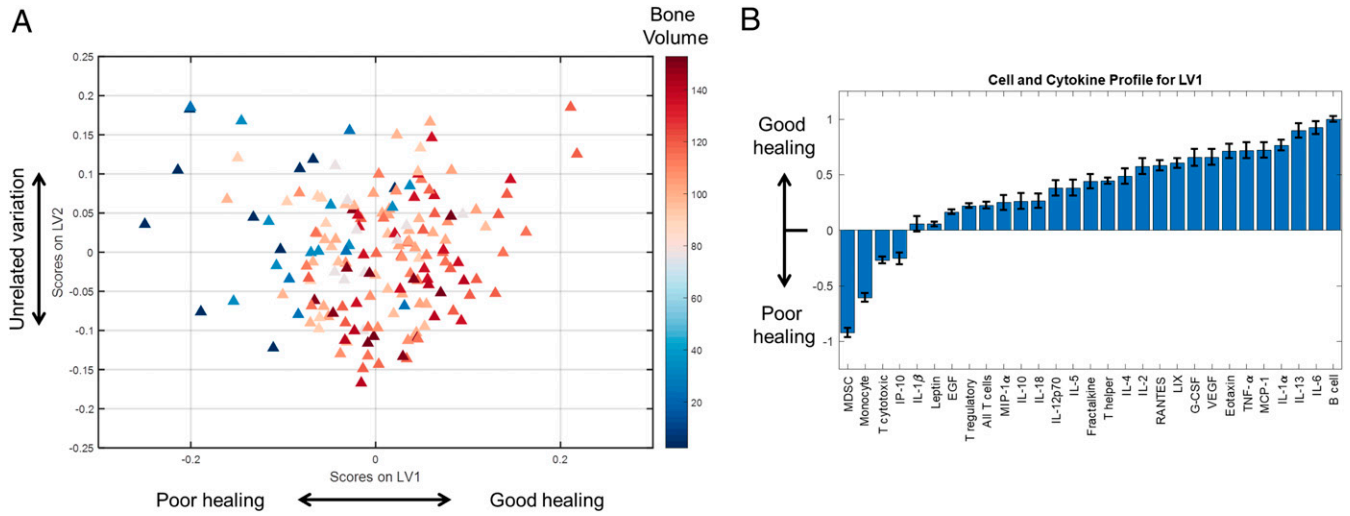

Fig. 4. PLSR of cell and cytokine data for all time points identifies the immune profile associated with healing. (*A*) The regression analysis established LV1, which describes samples along the continuum of healing responses. (*B*) LV1 defines the profile of immune cells and cytokines correlated with healing and shows that MDSCs, monocytes, cytotoxic T cells, and IP-10 were negatively correlated with healing while B cells, IL-6, IL-13, and IL-1α were positively correlated with healing.

Linear multivariate regression of all time points implicated IL-6 and IL-13 as the cytokines most positively correlated with bone formation, whereas IP-10 was the cytokine most negatively correlated with bone formation. These findings are consistent with previous reports that IL-6 stimulates angiogenesis and promotes callus mineralization (28, 29), while IL-13 inhibits bone resorption and enhances the alkaline phosphatase activity of osteoblasts (30, 31). In addition, IP-10 (also called CXCL10) has been associated with bone destruction by inducing osteoclast differentiation (32) and inhibiting angiogenesis (33). Interestingly, it has been shown that IP-10 is expressed by MDSCs in a murine cancer model (34) and furthermore, that plasma levels of IP-10 are correlated with MDSC frequency in a nonhuman primate model of viral infection (35), corroborating our findings that both IP-10 and MDSCs were highly negatively correlated with bone healing. Taken together with the immune cell data, these observations support our initial hypothesis that poor bone healing is associated with systemic immune dysregulation.

Next, we performed more in-depth analyses for the week 9 immune cell and cytokine data in an effort to identify early markers that potentially could be predictive of long-term bone healing outcomes. Conventional univariate regression as well as both linear and nonlinear multivariate analyses all demonstrated that MDSCs and IL-10 were unmistakable negative correlates of bone formation at this early time point. Using stochastic subsets of the week 9 data to generate nonlinear evolutionary models, we found that MDSCs and IL-10 were indeed the most influential biomarkers and could successfully be leveraged in a model ensemble to predict functional bone regeneration for the entire dataset. It is well established that MDSCs are among the major producers of immunosuppressive IL-10 (36–38), and that both factors are critical for the induction of T regulatory cells (24). Recent work has also shown that IL-10 has a reciprocal effect on MDSCs by promoting MDSC expansion during late-stage sepsis, which leads to enhanced and more detrimental immunosuppression (39). Our results suggest that elevated MDSC and IL-10 levels soon after trauma may be indicative of an aberrant early immunosuppressive response that can cascade into more severe long-term immune suppression and derail the normal bone healing response.

Overall, these results identify MDSCs and B cells as the most negative and positive, respectively, immune cell correlates for bone healing. Work from other groups has shown that B cells massively infiltrate the fracture callus soon after injury and differentiate into plasma cells that secrete large quantities of factors, including osteoprotegerin, which inhibits osteoclastogenesis and promotes fracture healing (40). Furthermore, B cells are critical for the production of high-quality bone, as the absence of mature B and T cells alters the matrix composition and results in stiffer and more brittle bones (41). In addition, there is evidence that MDSCs can directly suppress B cell differentiation, proliferation, and cytokine secretion (42–44). Therefore, the findings from our study provide further evidence that B cells play an important role in bone repair, and that the dynamic between B cells and MDSCs may be indicative of an overall proregenerative or antiregenerative response.

Regarding further characterization of MDSCs, we did confirm the presence of both granulocytic and monocytic populations by performing single-cell RNA-sequencing (scRNAseq) (*SI Appendix*, Fig. S4 *A–C*). scRNAseq also demonstrated that isolated MDSCs ($CD11b^+His48^+$ cells) expressed functional markers, including the genes encoding iNOS, arginase, and IL-1β (*SI Appendix*, Fig. S4*D*). Additional in vitro functional assessment of T cell suppression was performed by harvesting peripheral blood mononuclear cells (PBMCs) from naïve and trauma rats and culturing with or without $CD11b^+His48^+$ MDSCs isolated from the trauma rats. In this experiment, we found that T cell proliferation following CD3 and CD28 stimulation, including proliferation of $CD4^+$ and $CD8^+$ subsets, significantly decreased when MDSCs were added to the culture for both naïve and trauma PBMCs (*SI Appendix*, Fig. S5). These results demonstrate that MDSCs generated following traumatic injury remain functionally active and can directly suppress T cell proliferation.

It is important to acknowledge that correlation does not imply causation, and mechanistic experiments are still needed to validate the factors identified here as the predominant drivers of systemic immune dysregulation. Nonetheless, these results motivate future work to investigate how modulation of these cell populations and/or cytokines would influence bone healing. Other groups have begun exploring immunomodulatory strategies for enhancing bone repair by targeting macrophages (45) and T cells (46, 47) through the delivery of factors locally. However, there do not appear to be many examples in the literature that target B cells or MDSCs, particularly at the systemic level.

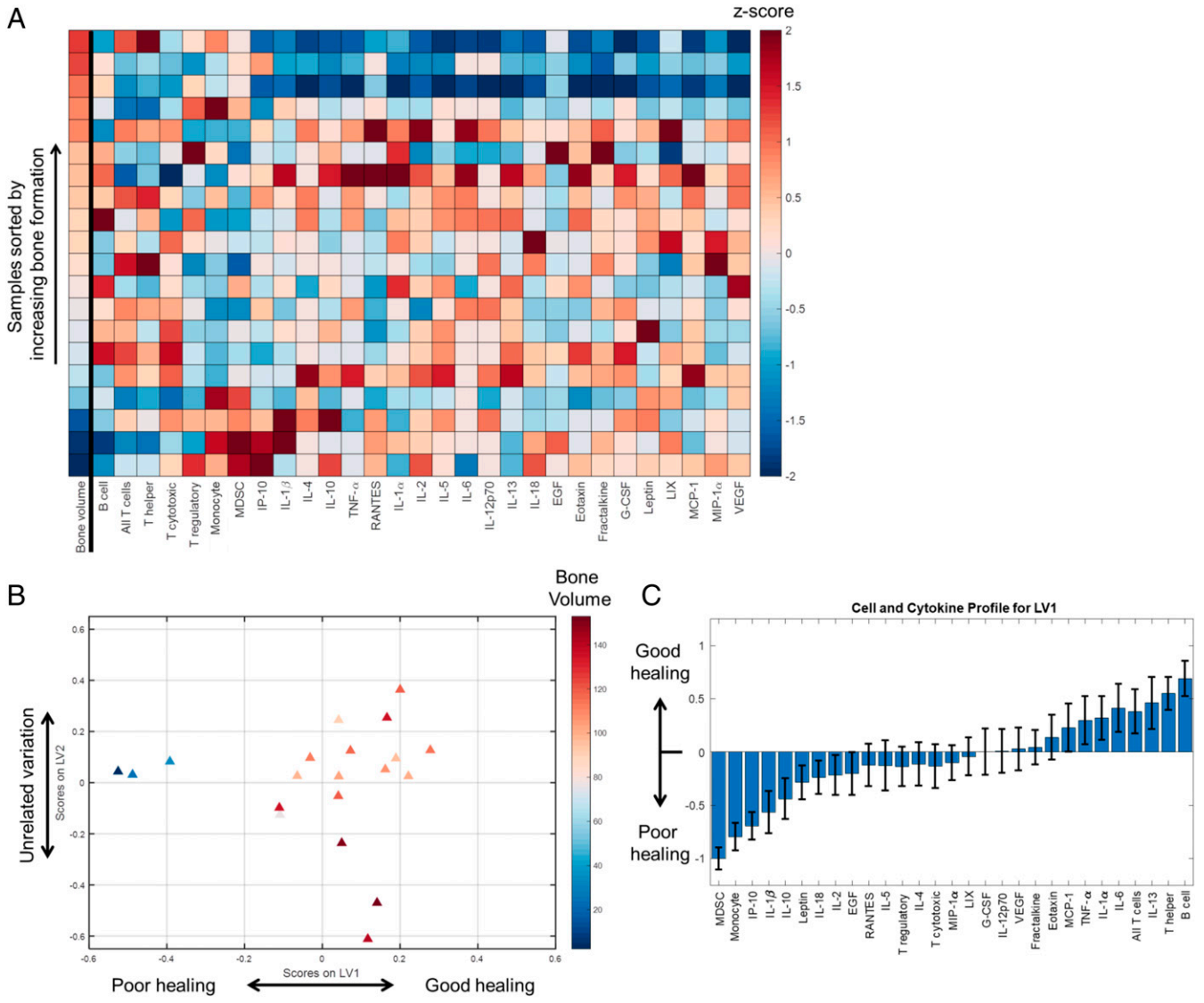

Fig. 5. PLSR of week 9 samples identifies early factors that are positively correlated and inversely correlated with healing. (*A*) Heatmap of *z*-scored week 9 immune cell and cytokine levels, sorted by week 20 bone volumes. (*B*) PLSR analysis established LV1, which describes samples along the continuum of healing responses. (*C*) This LV1 defines the profile of week 9 immune cells and cytokines correlated with healing and shows that MDSCs, monocytes, IP-10, and IL-1β were most negatively correlated with healing, while B cells, T helper cells, and IL-13 were most positively correlated with healing.

A potential limitation of this work is that the alterations observed in immune cell populations over time may have been affected by normal changes due to animal aging rather than just the response to trauma and subsequent treatment. In fact, immunosenescence with aging has been well documented (48, 49). One of the hallmarks is an overall reduction in T and B lymphocytes as hematopoietic progenitors gradually favor a shift toward myeloid lineage cells, particularly proinflammatory monocytes and macrophages (50, 51). However, many of these studies focus on age-related immune changes from childhood to geriatric age. In this study, all rats were 13 wk old at the start and 33 wk old at the terminal time point, which falls well within early adulthood for rats as they typically live around 2.5 to 3 y in captivity (52, 53). Consequently, we would expect age-related immune changes over the time course of this study to be minimal.

Despite these limitations, the results shown here provide significant insight into long-term immune profile changes following treatment of nonunion and demonstrate a link between systemic immune health and bone healing. Furthermore, this work establishes a viable framework for assessing multiple variable inputs (cells and cytokines measured from blood) to identify the most influential factors that may be predictive of a complex biological process such as bone repair. Additional work is needed to validate the predictive power of these computational models, and reproducibility in experiments with human clinical samples remains to be determined. Of note, recent clinical studies have taken a similar approach by analyzing serum/plasma from trauma patients and finding that levels of certain cytokines were associated with greater immune dysregulation and multiple organ dysfunction (54, 55). In that same vein, the results from this study can motivate further investigation into systemic immune profiles as a potentially powerful tool for early prediction of trauma healing outcomes.

In conclusion, in this study exploring the role of systemic immune dysregulation on healing in a rat model of chronic nonunion, our results show that delayed treatment of an established nonunion resulted in impaired bone healing compared to acute treatment. Although average levels of circulating immune cells and cytokines were not different between acute and delayed

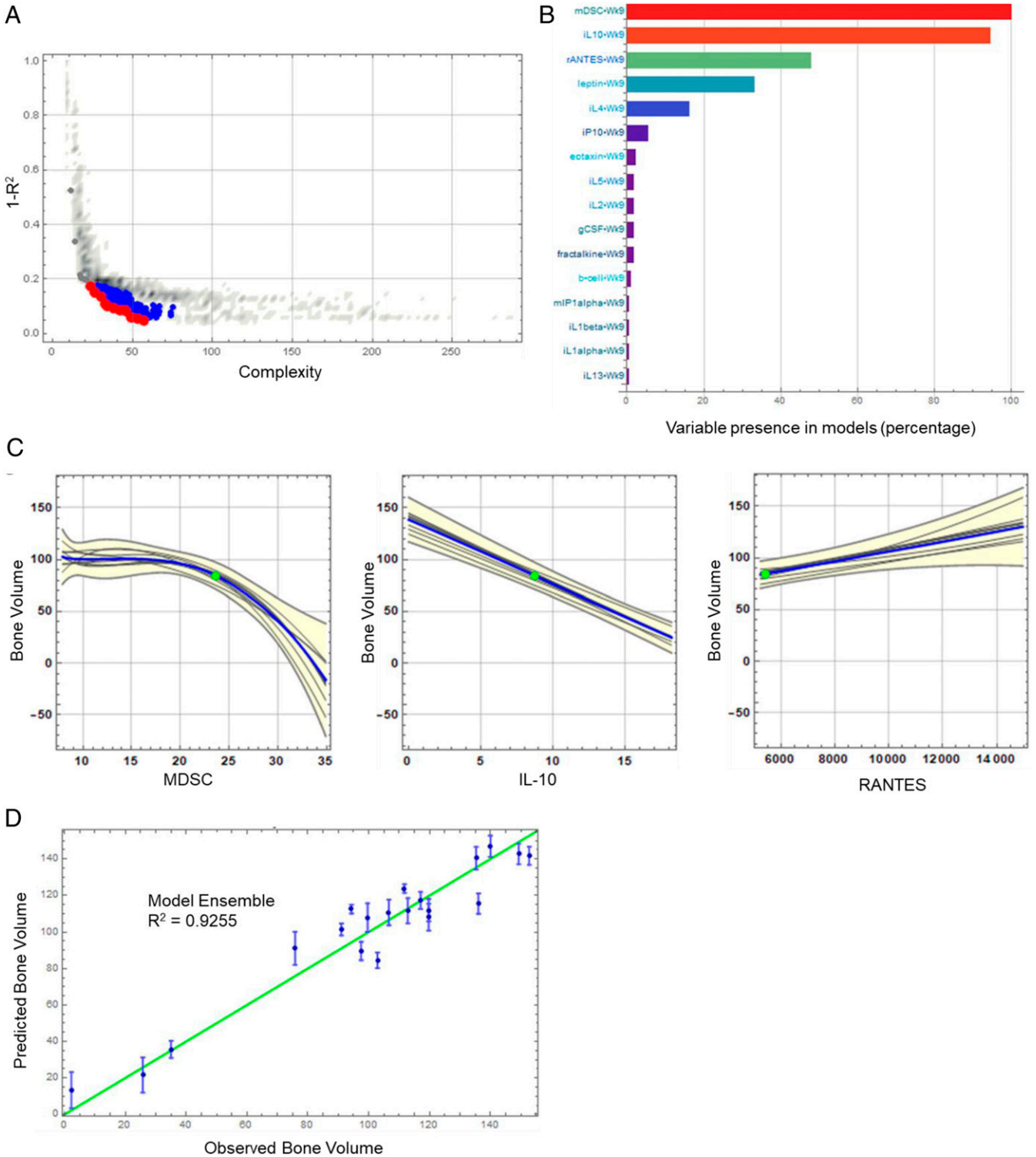

Fig. 6. Nonlinear multivariate analyses using Evolved Analytics DataModeler software supports MDSC and IL-10 as early negative predictors of bone healing. More than 1,100 unique models were generated using evolutionary symbolic regression algorithms. (*A*) The top 191 models were selected at the "knee" of the Pareto front, which represent the most accurate models with the lowest degree of complexity. (*B*) Variable presence chart showing MDSC, IL-10, and RANTES as most common variables in the selected models. (*C*) Response profile plots of the model ensemble for the top variable combination. The gray lines represent individual models, while the blue line represents the predictive model ensemble (aggregate of the top nine individual models). The yellow envelopes demonstrate the variance in the ensemble as a function of each variable. (*D*) Model ensemble prediction plot demonstrating high predictive power of the model ensemble for the observed data. This can be seen by how closely the data points lie to the green line (a representation of 100% model ensemble prediction accuracy). The error bars around each data point illustrate the spread of the ensemble predictions.

treatment groups overall, univariate and multivariate regression modeling revealed significant correlations between early cell and cytokine biomarkers and functional bone regeneration. Elevated circulating levels of MDSCs, IP-10, and IL-10 were all inversely correlated with healing, whereas B cells, T helper cells, IL-6, and IL-13 were positively correlated. Some of these correlations, MDSCs and IL-10, were significant as early as 1 wk posttreatment, as determined through univariate and multivariate analyses. Taken together, these results suggest that MDSCs and long-term immune dysregulation play a key role in impaired healing after nonunion and could potentially serve as novel therapeutic targets to enhance bone repair.

Materials and Methods

Experimental Design. The objective of this study was to investigate whether the early systemic immune response following traumatic injury in a recently established animal model of nonunion (25) could be predictive of long-term bone regeneration. We set up the in vivo study as described below and collected blood samples at multiple time points to perform ex vivo cell and proteomic analyses. Concurrently, noninvasive imaging techniques (radiography/μCT) were used to evaluate bone formation over time. At the final time point, terminal mechanical testing was performed to functionally assess the regenerated bones. Sample numbers for each experiment were determined using power analyses based on input from previous studies, and are noted in the figure legends. All animals and treatment groups were assigned at random, and investigators were blinded for all in vivo and ex vivo analyses.

Alginate BMP-2 Preparation. Arginine-glycine-aspartic acid (RGD)-functionalized alginate (FMC BioPolymer) was reconstituted in MEM α medium (Thermo Fisher Scientific) to create a 2% wt/vol solution, as described previously (56). Recombinant human BMP-2 (Pfizer) was reconstituted in a solution of 0.1% rat serum albumin (Sigma-Aldrich) in 4 mM hydrochloric acid and mixed with the alginate solution to yield 2 μg BMP-2 per 150 μL of final solution. This alginate/BMP-2 solution was gelled with the addition of calcium sulfate (Sigma-Aldrich) at a 1:25 volume ratio. Hydrogels were prepared under sterile conditions inside a laminar flow hood and stored overnight at 4 °C before use in surgery the next day.

Animal Model. For these studies, 13-wk-old female SASCO Sprague–Dawley rats (Charles River Laboratories) were used. Rats were pair-housed in individually ventilated caging (Tecniplast) with a tunnel and gnawing blocks (Bio-Serv) for enrichment. Bedding was a mixture of corn cob and processed paper. Chow (Purina Mills International #5001) was fed ad libitum. Filtered tap water treated with UV light was provided ad libitum in bottles. Sentinel results from Charles River Laboratories PCR Rodent Infectious Agent testing were negative for all pathogens in the housing room. All animals were allowed to acclimate for at least 2 wk before any procedures were performed. Following each procedure, a divider was temporarily placed in the cage for better monitoring of postoperative recovery. Animals were randomly allocated to treatment groups.

Surgical Procedures. All surgical procedures were approved by the Georgia Institute of Technology's Institutional Animal Care and Use Committee. Anesthesia was induced and maintained using isoflurane (Henry Schein Animal Health) inhalation. Prior to each procedure, all animals were given a subcutaneous injection of sustained-release buprenorphine (ZooPharm) for analgesia. Briefly, an anterolateral skin incision was made in the thigh, followed by blunt dissection to separate the overlaying muscles to reach the femur. Limited extension of this muscle window allowed for placement of a radiolucent polysulfone fixation plate for internal stabilization. Critically sized 8-mm defects were created in the mid-diaphysis of the femur using an oscillating saw. For the acutely-treated animals, a 6-mm diameter polycaprolactone (PCL) nanofiber mesh (Sigma-Aldrich) was carefully placed around the newly exposed bone ends, and alginate loaded with BMP-2 was delivered via syringe injection through the mesh perforations. Subsequently the muscle and skin were closed using 4-0 Vicryl suture and wound clips, respectively. In contrast, for the animals receiving delayed treatment, the bone defects were initially left empty (no treatment), and the muscle and skin were closed. At 8 wk, a second procedure was performed on these animals where the original incision was reopened to expose the fixation plate and femur. An oscillating saw was used to remove any mineralized end capping of the defects and any soft tissue ingrowth within the defect space was cleared to allow for placement of the PCL nanofiber mesh. Finally, alginate/BMP-2 was delivered, and the muscle and skin were closed as before.

Radiography and μCT. To qualitatively assess longitudinal bone regeneration, two-dimensional in vivo digital radiographs were acquired with an MX-20 digital X-ray system (Faxitron) at 2, 4, 8, and 12 wk posttreatment. Longitudinal bone formation was quantitatively evaluated using three-dimensional μCT at 6 and 12 wk posttreatment. In vivo scans of the harvested femora were performed before mechanical testing using the vivaCT40 (Scanco Medical) at a 38-μm voxel size, 55-kVp voltage, and a 145-μA current. A threshold corresponding to 50% of native cortical bone density was applied to segment bone mineral and identify newly regenerated bone, as established previously (56). The volume of interest consisted of the central 6.46 mm (170 slices) of the 8-mm defect.

Biomechanical Testing. Torsional testing to failure was performed as previously described (56). Femurs were excised at week 20 (12 wk posttreatment), wrapped in PBS-soaked gauze, and stored at −20 °C until testing could be performed. On the day of testing, samples were thawed, the surrounding soft tissues were excised, and the femora were first μCT-scanned, as described above. Subsequently, the fixation plate was removed so that the native bone ends could be potted in Wood's metal (Alfa Aesar). The potted femurs were tested to failure in torsion at a rotation rate of 3°/s using the EnduraTEC ELF3200 axial/torsion testing system (Bose). Failure strength was determined by locating the peak torque within the first 60° of rotation. Torsional stiffness was calculated by finding the slope of the linear region before failure in the torque-rotation plot.

Tissue Collection and Processing. Blood was collected longitudinally via the rat tail vein at 0 (baseline), 1, 2, 4, 8, 9, 10, 12, 16, and 20 wk into two fractions: one for whole blood and the other for serum in the appropriate Microvette collection tubes (Kent Scientific). For serum isolation, tubes were allowed to clot at room temperature for 30 min before being stored at 4 °C overnight. The next day, all serum tubes were centrifuged at 1,500 × *g* for 10 min, and the yellow (straw) serum was collected and stored at −20 °C.

The spleen, bone marrow from the left tibia, and muscle adjacent to the defect were all harvested at the endpoint (week 20). Red blood cells were lysed in all samples using 1× RBC Lysis Buffer (eBioscience) according to the manufacturer's instructions. Following lysis, cells were fixed using Cytofix fixation buffer (BD Biosciences), resuspended in FACS buffer containing 2% fetal bovine serum (FBS) in 1× phosphate-buffered saline (PBS), and stored at 4 °C until staining for flow cytometry.

Luminex Multiplex Array and Flow Cytometry. Serum isolates collected at all time points were analyzed for cytokines using the Milliplex MAP Rat Cytokine/Chemokine Magnetic Bead Panel (Millipore Sigma). The assays were read using a MAGPIX Luminex instrument (Luminex), and the median fluorescent intensity values read by the machine (with background subtracted) were recorded.

Processed whole blood samples were stained for flow cytometry analysis. Prior to staining, cells with Fc receptors were blocked with purified mouse anti-rat CD32 (BD Biosciences) for 10 min at 4 °C to prevent nonspecific binding. Cells were then stained for various immune cell populations, including T cells ($CD3^+$), T helper cells ($CD3^+CD4^+$), cytotoxic T cells ($CD3^+CD8^+$), T regulatory cells ($CD3^+CD4^+FoxP3^+$), myeloid-derived suppressor cells ($His48^+CD11b^+$), B cells ($B220^+$), and monocytes ($CD68^+$, Bio-Rad) with specific anti-rat antibodies (eBioscience, unless otherwise noted). Sample data were collected using a BD Accuri C6 flow cytometer and analyzed using FlowJo software. Gates were positioned based on fluorescence minus one controls with <1% noise allowed.

Linear Multivariate Analyses. Cytokine and immune cell data for each time point were compiled. PLSR was conducted in MATLAB (MathWorks) using the partial least squares algorithm of Cleiton Nunes (available on the MathWorks File Exchange). The data were *z*-scored (mean subtracted and normalized to SD for each cytokine) before being passed into the algorithm. This multivariate method requires scale-free data so that the analysis would not be biased toward variables with extremely high values. An orthogonal rotation in the LV1-LV2 plane was used to define the axis that best matched the continuum of healing responses (week 20 bone volume). A Monte Carlo subsampling using 1,000 iterations was used to characterize SD on the individual signals involved in LV1 of the PLSR model. For each iteration, 85% (17/20) of the samples used to construct the total PLSR model were sampled at random, and a new PLSR model was constructed. To correct for sign reversals, each subsampled LV1 was multiplied by the sign of the scalar product

of the new LV1 and the corresponding LV1 from the total model. The same orthogonal rotation used for the total model was applied to the LV1s from each iteration, and the mean and SD were computed for each signal across all iterations.

Nonlinear Multivariate Analyses. Nonlinear regression was performed using Evolved Analytics DataModeler software to further investigate cytokine and immune cell correlations with bone volume. Nonlinear algebraic models from 20 independent evolutions were generated using DataModeler's SymbolicRegression function, which utilizes evolutionary symbolic algorithms. These models were then plotted as a function of fit ($1 - R^2$) and complexity. Next, 191 models with complexity <80 and a $1 - R^2$ value <0.175 were selected as the "fittest" models, which represent the models with the optimal balance of fit (R^2) and complexity observed at the knee of the Pareto front. These selected models were then analyzed using the VariablePresence and VariableCombinations functions to identify the dominant variables and variable combinations. Finally, the models involving the top variable combination were identified and aggregated into a model ensemble using the VariablePresence and CreateModelEnsemble functions, respectively. The resulting model ensemble is composed of all the generated models for the chosen variable combination and defines a predictive model that best fits the imported dataset. This model ensemble was further evaluated using the ResponsePlotExplorer function to visualize the response of bone volume as a function of each individual variable within the ensemble.

scRNAseq. For cell isolation, whole blood was collected via the rat tail vein from trauma rats, as previously described (57), and MDSCs were sorted via magnetic-activated cell sorting (Miltenyi Biotec) using His48 according to manufacturer's instructions. FACS analysis following cell sorting confirmed >85% $CD11b^+His48^+$ MDSCs.

Next, the cells were spun down and washed immediately after being diluted in 10 mL of PBS + 0.1% BSA. The samples were then processed through a cell strainer to filter out any debris and cell clumps. The cells were counted for each sample using Cellometer (Nexcelom) and NucleoCounter (Chemometec) automated cell counters to check the targeted cell number and viability. The volume was optimized to achieve the target of 5,000 barcoded cells. scRNAseq was performed using Single Cell 3′ Solution v3.1 (10X Genomics), according to the manufacturer's instructions (protocol rev C). Libraries were sequenced on a NextSeq 500 system (Illumina).

The data were de-multiplexed, aligned, and counted using Cell Ranger version 3.1.0 (10X Genomics). Samples were analyzed by Seurat (https://satijalab.org/seurat/) using canonical correction analysis with Louvain clustering and visualized by *t*-distributed stochastic neighbor embedding projections. Quality control metrics were used to select cells with a mitochondrial gene percentage <10% and filter cells with unique feature counts >2,500 or <200. These include the selection and filtration of cells based on quality control metrics, data normalization and scaling, and detection of highly variable features.

T Cell Immunosuppression Assay. Whole blood was collected via the rat tail vein from four trauma rats and three healthy rats as previously described (57). Red blood cells were removed using 1× RBC lysis buffer (eBioscience). Cells were rinsed twice with 1× PBS, and MDSCs were sorted out of the trauma rat cells by magnetic-activated cell sorting (Miltenyi Biotec) using His48 according to the manufacturer's instructions. The MDSC fraction and the remaining PBMC fraction were saved. The PBMC fraction from the trauma rats (trauma − MDSCs) and PBMCs from the healthy rats (naïve) were plated in separate tissue culture plates treated with 5 μg/mL immobilized anti-rat CD3 and 0.5 μg/mL soluble CD28 (BioLegend). A third group and fourth group were also plated that contained the MDSC and PBMC fractions from the trauma rats in a 1:1 ratio (trauma + MDSCs) or MDSCs from the trauma rats and PBMCs from the healthy rats in a 1:1 ratio (naïve + MDSCs). Cells were incubated for 16 h, after which 10 μM BrdU was added to each well. After 24 h, cells were collected and stained for CD3, CD4, CD8, and BrdU. Surface antigens were stained as previously described prior to BrdU staining. After surface antigen staining, cells were permeabilized with Cytoperm Permeabilization Buffer Plus (BD Biosciences) according to the manufacturer's instructions. Cells were then treated with 300 μg/mL DNase for 1 h at 37 °C and then washed in 1× BD Perm/Wash Buffer (BD Biosciences). Cells were then stained with anti-BrdU APC (BioLegend) and analyzed via flow cytometry.

Statistical Analyses. All data are reported as mean ± SEM. Significance was determined using the *t* test or ANOVA as appropriate, with multiple comparisons done using Tukey's post hoc test. Significance was determined at $P < 0.05$. All statistical calculations were performed using GraphPad Prism 7 software. Sample sizes were determined by performing a power analysis in G*Power software based on bone volume and maximum torque results obtained from previous studies. These power calculations, along with historical data using this segmental bone defect rat model, suggested that a sample size of seven or eight was sufficient to provide statistical differences between groups.

Data Availability. All data are included in the main text and *SI Appendix*.

ACKNOWLEDGMENTS. We thank Boao Xia, Hazel Stevens, Angela Lin, Ramesh Subbiah, Brennan Torstrick, Brett Klosterhoff, Olivia Burnsed, Giuliana Salazar-Noratto, Jason Wang, Ryan Akman, Lina Mancipe Castro, and Gilad Doron for their assistance with surgeries and various experiments, as well as Paramita Chatterjee for her scRNA sequencing expertise. We also thank the core facilities at the Parker H. Petit Institute for Bioengineering and Bioscience at the Georgia Institute of Technology for the use of their shared equipment, services, and expertise. This work was supported by the AFIRM II (US Armed Forces Institute of Regenerative Medicine) effort (Award W81XWH-14-2-0003) and a National Institutes of Health R01 grant (R01AR074960). The US Army Medical Research Acquisition Activity was the awarding and administering acquisition office. The opinions, interpretations, conclusions, and recommendations in this paper are those of the authors and are not necessarily endorsed by the Department of Defense.

1. A. L. Dougherty *et al*., Battlefield extremity injuries in operation Iraqi freedom. *Injury* **40**, 772–777 (2009).
2. M. Banerjee *et al*., German Trauma Registry Group, Epidemiology of extremity injuries in multiple trauma patients. *Injury* **44**, 1015–1021 (2013).
3. R. Zura *et al*., Epidemiology of fracture nonunion in 18 human bones. *JAMA Surg.* **151**, e162775 (2016).
4. A. M. Harris, P. L. Althausen, J. Kellam, M. J. Bosse, R. Castillo; Lower Extremity Assessment Project (LEAP) Study Group, Complications following limb-threatening lower extremity trauma. *J. Orthop. Trauma* **23**, 1–6 (2009).
5. S. Flohé, S. B. Flohé, F. U. Schade, C. Waydhas, Immune response of severely injured patients—influence of surgical intervention and therapeutic impact. *Langenbecks Arch. Surg.* **392**, 639–648 (2007).
6. F. Kimura, H. Shimizu, H. Yoshidome, M. Ohtsuka, M. Miyazaki, Immunosuppression following surgical and traumatic injury. *Surg. Today* **40**, 793–808 (2010).
7. S. K. Tschoeke, W. Ertel, Immunoparalysis after multiple trauma. *Injury* **38**, 1346–1357 (2007).
8. J. M. Lord *et al*., The systemic immune response to trauma: An overview of pathophysiology and treatment. *Lancet* **384**, 1455–1465 (2014).
9. A. M. Binkowska, G. Michalak, R. Słotwiński, Current views on the mechanisms of immune responses to trauma and infection. *Cent. Eur. J. Immunol.* **40**, 206–216 (2015).
10. M. D. Rosenthal, F. A. Moore, Persistent inflammation, immunosuppression, and catabolism: Evolution of multiple organ dysfunction. *Surg. Infect. (Larchmt.)* **17**, 167–172 (2016).
11. W. Xiao *et al*.; Inflammation and Host Response to Injury Large-Scale Collaborative Research Program, A genomic storm in critically injured humans. *J. Exp. Med.* **208**, 2581–2590 (2011).
12. M. D. Rosenthal, F. A. Moore, Persistent inflammatory, immunosuppressed, catabolic syndrome (PICS): A new phenotype of multiple organ failure. *J. Adv. Nutr. Hum. Metab.* **1**, e784 (2015).
13. C. E. Vantucci, K. Roy, R. E. Guldberg, Immunomodulatory strategies for immune dysregulation following severe musculoskeletal trauma. *J. Immunol. Regen. Med.* **2**, 21–35 (2018).
14. L. F. Gentile *et al*., Persistent inflammation and immunosuppression: A common syndrome and new horizon for surgical intensive care. *J. Trauma Acute Care Surg.* **72**, 1491–1501 (2012).
15. V. P. Makarenkova, V. Bansal, B. M. Matta, L. A. Perez, J. B. Ochoa, $CD11b^+/Gr\text{-}1^+$ myeloid suppressor cells cause T cell dysfunction after traumatic stress. *J. Immunol.* **176**, 2085–2094 (2006).
16. B. Mathias *et al*.; the Sepsis, Critical Illness Research Center Investigators, Human myeloid-derived suppressor cells are associated with chronic immune suppression after severe sepsis/septic shock. *Ann. Surg.* **265**, 827–834 (2017).
17. D. I. Gabrilovich, S. Nagaraj, Myeloid-derived suppressor cells as regulators of the immune system. *Nat. Rev. Immunol.* **9**, 162–174 (2009).
18. W. Jia, C. Jackson-Cook, M. R. Graf, Tumor-infiltrating, myeloid-derived suppressor cells inhibit T cell activity by nitric oxide production in an intracranial rat glioma + vaccination model. *J. Neuroimmunol.* **223**, 20–30 (2010).
19. C. Zhang *et al*., Accumulation of myeloid-derived suppressor cells in the lungs during Pneumocystis pneumonia. *Infect. Immun.* **80**, 3634–3641 (2012).
20. P. Raber, A. C. Ochoa, P. C. Rodríguez, Metabolism of L-arginine by myeloid-derived suppressor cells in cancer: mechanisms of T cell suppression and therapeutic perspectives. *Immunol. Invest.* **41**, 614–634 (2012).
21. R. Geiger *et al*., L-arginine modulates T cell metabolism and enhances survival and anti-tumor activity. *Cell* **167**, 829–842.e13 (2016).
22. H. Li, Y. Han, Q. Guo, M. Zhang, X. Cao, Cancer-expanded myeloid-derived suppressor cells induce anergy of NK cells through membrane-bound TGF-beta 1. *J. Immunol.* **182**, 240–249 (2009).

23. T. Condamine, D. I. Gabrilovich, Molecular mechanisms regulating myeloid-derived suppressor cell differentiation and function. *Trends Immunol.* **32**, 19–25 (2011).
24. M. J. Park *et al*., Interleukin-10 produced by myeloid-derived suppressor cells is critical for the induction of Tregs and attenuation of rheumatoid inflammation in mice. *Sci. Rep.* **8**, 3753 (2018).
25. A. Cheng *et al*., Impaired bone healing following treatment of established nonunion correlates with serum cytokine expression. *J. Orthop. Res.* **37**, 299–307 (2018).
26. S. Morshed, Current options for determining fracture union. *Adv. Med.* **2014**, 708574 (2014).
27. E. J. Wherry, M. Kurachi, Molecular and cellular insights into T cell exhaustion. *Nat. Rev. Immunol.* **15**, 486–499 (2015).
28. R. Marsell, T. A. Einhorn, The biology of fracture healing. *Injury* **42**, 551–555 (2011).
29. X. Yang *et al*., Callus mineralization and maturation are delayed during fracture healing in interleukin-6 knockout mice. *Bone* **41**, 928–936 (2007).
30. A. Frost *et al*., Interleukin (IL)-13 and IL-4 inhibit proliferation and stimulate IL-6 formation in human osteoblasts: Evidence for involvement of receptor subunits IL-13R, IL-13Ralpha, and IL-4Ralpha. *Bone* **28**, 268–274 (2001).
31. Y. Onoe *et al*., IL-13 and IL-4 inhibit bone resorption by suppressing cyclooxygenase-2-dependent prostaglandin synthesis in osteoblasts. *J. Immunol.* **156**, 758–764 (1996).
32. E. Y. Lee, Z. H. Lee, Y. W. Song, CXCL10 and autoimmune diseases. *Autoimmun. Rev.* **8**, 379–383 (2009).
33. A. L. Angiolillo *et al*., Human interferon-inducible protein 10 is a potent inhibitor of angiogenesis in vivo. *J. Exp. Med.* **182**, 155–162 (1995).
34. N. Umemura *et al*., Tumor-infiltrating myeloid-derived suppressor cells are pleiotropic-inflamed monocytes/macrophages that bear M1- and M2-type characteristics. *J. Leukoc. Biol.* **83**, 1136–1144 (2008).
35. S. E. Dross *et al*., Kinetics of myeloid-derived suppressor cell frequency and function during simian immunodeficiency virus infection, combination antiretroviral therapy, and treatment interruption. *J. Immunol.* **198**, 757–766 (2017).
36. K. M. Hart, K. T. Byrne, M. J. Molloy, E. M. Usherwood, B. Berwin, IL-10 immunomodulation of myeloid cells regulates a murine model of ovarian cancer. *Front. Immunol.* **2**, 29 (2011).
37. M. L. Ibrahim *et al*., Myeloid-derived suppressor cells produce IL-10 to elicit DNMT3b-dependent IRF8 silencing to promote colitis-associated colon tumorigenesis. *Cell Rep.* **25**, 3036–3046.e6 (2018).
38. L. Brudecki, D. A. Ferguson, C. E. McCall, M. El Gazzar, Myeloid-derived suppressor cells evolve during sepsis and can enhance or attenuate the systemic inflammatory response. *Infect. Immun.* **80**, 2026–2034 (2012).
39. I. Bah, A. Kumbhare, L. Nguyen, C. E. McCall, M. El Gazzar, IL-10 induces an immune repressor pathway in sepsis by promoting S100A9 nuclear localization and MDSC development. *Cell. Immunol.* **332**, 32–38 (2018).
40. I. Könnecke *et al*., T and B cells participate in bone repair by infiltrating the fracture callus in a two-wave fashion. *Bone* **64**, 155–165 (2014).
41. T. El Khassawna *et al*., T lymphocytes influence the mineralization process of bone. *Front. Immunol.* **8**, 562 (2017).
42. J. Jaufmann *et al*., Human monocytic myeloid-derived suppressor cells impair B-cell phenotype and function in vitro. *Eur. J. Immunol.* **50**, 33–47 (2020).
43. B. Knier *et al*., Myeloid-derived suppressor cells control B cell accumulation in the central nervous system during autoimmunity. *Nat. Immunol.* **19**, 1341–1351 (2018).
44. Y. Wang *et al*., Myeloid-derived suppressor cells impair B cell responses in lung cancer through IL-7 and STAT5. *J. Immunol.* **201**, 278–295 (2018).
45. K. L. Spiller *et al*., Sequential delivery of immunomodulatory cytokines to facilitate the M1-to-M2 transition of macrophages and enhance vascularization of bone scaffolds. *Biomaterials* **37**, 194–207 (2015).
46. S. Reinke *et al*., Terminally differentiated $CD8^+$ T cells negatively affect bone regeneration in humans. *Sci. Transl. Med.* **5**, 177ra36 (2013).
47. Y. Liu *et al*., Mesenchymal stem cell-based tissue regeneration is governed by recipient T lymphocytes via IFN-γ and TNF-α. *Nat. Med.* **17**, 1594–1601 (2011).
48. K. Dorshkind, E. Montecino-Rodriguez, R. A. Signer, The ageing immune system: Is it ever too old to become young again? *Nat. Rev. Immunol.* **9**, 57–62 (2009).
49. E. Montecino-Rodriguez, B. Berent-Maoz, K. Dorshkind, Causes, consequences, and reversal of immune system aging. *J. Clin. Invest.* **123**, 958–965 (2013).
50. P. J. Linton, K. Dorshkind, Age-related changes in lymphocyte development and function. *Nat. Immunol.* **5**, 133–139 (2004).
51. A. C. Shaw, S. Joshi, H. Greenwood, A. Panda, J. M. Lord, Aging of the innate immune system. *Curr. Opin. Immunol.* **22**, 507–513 (2010).
52. D. V. Agoston, How to translate time? The temporal aspect of human and rodent biology. *Front. Neurol.* **8**, 92 (2017).
53. N. A. Andreollo, E. F. Santos, M. R. Araújo, L. R. Lopes, Rat's age versus human's age: What is the relationship? *Arq. Bras. Cir. Dig.* **25**, 49–51 (2012).
54. M. Braunstein *et al*., Polytrauma in older adults leads to significantly increased TIMP-1 levels in the early posttraumatic period. *J. Immunol. Res.* **2020**, 4936374 (2020).
55. G. E. Gaski *et al*., Early immunologic response in multiply injured patients with orthopaedic injuries is associated with organ dysfunction. *J. Orthop. Trauma* **33**, 220–228 (2019).
56. Y. M. Kolambkar *et al*., An alginate-based hybrid system for growth factor delivery in the functional repair of large bone defects. *Biomaterials* **32**, 65–74 (2011).
57. C. E. Vantucci *et al*., Development of systemic immune dysregulation in a rat trauma model of biomaterial-associated infection. *Biomaterials* **264**, 120405 (2021).